Published in final edited form as:
Int J Appl Earth Obs Geoinf. 2012 April 1; 15: 49–56. doi:10.1016/j.jag.2011.06.003.

Frequency distribution signatures and classification of within-object pixels

Douglas A. Stow[*], **Sory I. Toure**, **Christopher D. Lippitt**, **Caitlin L. Lippitt**, and **Chung-rui Lee**
Department of Geography, San Diego State University, 5500 Campanile Drive, San Diego, CA, 92182-4493, USA

Abstract

The premise of geographic object-based image analysis (GEOBIA) is that image objects are composed of aggregates of pixels that correspond to earth surface features of interest. Most commonly, image-derived objects (segments) or objects associated with predefined land units (e.g., agricultural fields) are classified using parametric statistical characteristics (e.g., mean and standard deviation) of the within-object pixels. The objective of this exploratory study was to examine the between- and within-class variability of frequency distributions of multispectral pixel values, and to evaluate a quantitative measure and classification rule that exploits the full pixel frequency distribution of within object pixels (i.e., histogram signatures) compared to simple parametric statistical characteristics. High spatial resolution Quickbird satellite multispectral data of Accra, Ghana were evaluated in the context of mapping land cover and land use and socioeconomic status. Results show that image objects associated with land cover and land use types can have characteristic, non-normal frequency distributions (histograms). Signatures of most image objects tended to match closely the training signature of a single class or sub-class. Curve matching approaches to classifying multi-pixel frequency distributions were found to be slightly more effective than standard statistical classifiers based on a nearest neighbor classifier.

Keywords

object classification; curve matching; QuickBird; land cover; land use; Ghana

1. Introduction

The main premise of geographic object-based image analysis (GEOBIA) is that image objects are composed of pixel groupings that correspond to earth surface features of interest (Blaschke, 2009; Hay and Castilla, 2008.). For most implementations of GEOBIA, pixel groups are first delineated through image segmentation (Burnett and Blaschke, 2003; Schiewe, 2002) or extant field or land parcel boundaries, and then within-segment pixels are classified in aggregate. Classification decisions are normally based on parametric statistical measures of central tendency (e.g., mean or median) (Shackelford and Davis, 2003) and/or dispersion (e.g., standard deviation or range) (Pedley and Curran, 1991) for within-segment pixels. However, the frequency distributions of image brightness values for within-object

[*]Corresponding author: stow@mail.sdsu.edu; 01-619-594-5498.

pixels may be complex and not normally distributed, such that the mean and standard deviation measures may not be effective or appropriate measures of central tendency or dispersion.

The emphasis of this study is on the second phase of GEOBIA, the classification of multi-pixel groups associated with an image object. The use of histogram curve matching techniques to quantify the similarity between image objects is explored and compared to traditional parametric descriptors. GEOBIA classification assumes that some form of object delineation has already been performed. Delineation typically occurs through image segmentation, for which a variety of approaches to forming image objects have been developed (Dey et al., 2010; Haralick and Shapiro, 1985; Neubert et al., 2008). Field-based image classification approaches utilize extent land boundary files such as agricultural field or urban land ownership parcels, as the basis of object delineation. Per-field classification approaches have been utilized for over three decades (Landgrebe, 1980; Mason et al., 1988), however classification decisions are typically based on statistical characteristics of the within-field pixels (Dean and Smith, 2003) or a per-pixel classification of the input multispectral image data (Shandley et al., 1996; Woodcock and Harward, 1992). Berberoglu et al. (2000) tested pixel- and per-field approaches to image classification and found that the latter was more successful, by exploiting the variability in spatial frequencies of land cover types. Even for segments/objects with normal distributions, using only mean and/or standard deviation may not fully capture signatures of within-segment pixels (Lloyd et al., 2004). Also, the shapes of image brightness histograms of within-object pixels for certain types of land cover and land use classes may be characteristic or diagnostic (i.e., characteristic shape signatures).

While we find no published work pertaining to the use of histogram curve matching approaches to classifying image segments in the GEOBIA literature, similar approaches are evident in computer vision and image understanding literature. Histogram matching is commonly used for relative radiometric normalization of multi-temporal images (Coulter et al., 2009) and for template matching for shape recognition in computer vision research (Cheng and Chen, 2003; Zhang et al., 2006).

Curve matching techniques used for hyperspectral classification may be useful for classification of within-segment pixel frequency distributions. Curve matching techniques are used to measure spectral similarity between a known spectrum from a spectral library with unknown image pixel/object spectra (Kruse et al., 1993; van der Meer, 2006) and may be applicable to quantifying the similarity between histogram curves representing within-object pixels.

The objectives of this study were to: (1) examine within- and between-class variability of frequency distributions of multispectral DN values of within-segment pixels to determine if within-class histogram curves are similar and between-class curves are separable, and (2) evaluate a quantitative measure and classification approach that exploits characteristic frequency distributions (i.e., histogram signatures) of within-segment pixels. The application context for this evaluation is the classification and mapping of general land cover/land use (LCLU) types and socio-economic status (SES) of residential areas within Accra, Ghana, based on satellite multispectral image data having high spatial resolution. The goals of this exploratory study are to assess whether LCLU types appear to have characteristic frequency distribution signatures and subsequently, whether curve matching based on such frequency distribution signatures hold promise for the classification phase of OBIA. We take a per-field approach to this evaluation, by starting with the delineated polygon boundaries that represent LCLU objects and then examine the frequency distributions of pixels belonging to those objects.

2. Study Area and Data

The study area is a portion of the Accra, Ghana metropolitan area, which is delineated in Figure 1. Accra is the capital city of around two million people and has grown rapidly in the last decade (Ghana Statistical Services, 2002). Our on-going studies of demographic and health survey data attempt to integrate fine spatial resolution satellite data to assess spatial variations in poverty and health within Accra, Ghana (Weeks et al., 2006; Weeks et al., 2007). For studies of urban health, it is important to know where a city's inhabitants reside, and LCLU may be important for determining sources or vectors of disease. No comprehensive or reliable source of LCLU data exists for Accra. A majority of Accra's inhabitants are poor and live in low SES neighborhoods, and there is a need to further identify SES for LCLU polygons mapped as residential land use. The abundance of vegetation cover and size of building structures indicate differences in SES of residential areas (Lippitt et al., in press; Stow et al., 2007; Stow et al., 2010).

A general, five-category LCLU classification scheme is utilized in this study and is driven by the applications context described previously. This classification scheme includes the following LCLU classes: (1) Low Socio-economic (LSE) Residential, (2) High Socioeconomic (HSE) Residential, (3) Urban Non-residential, (4) Urban Agriculture, and (5) Forest/Natural Vegetation, as described in Table 1. Urban Non-residential is a highly generalized class consisting of several built land use types and our application needs are such that these individual LCLU types need not be identified and mapped as separate categories. While this simplifies the classification scheme and mapping, these various LCLU subclasses can have unique brightness histogram signatures that should be represented separately in the training and curve matching phases of the GEOBIA classification process. Also, categories such as High Socioeconomic Residential and Urban Agriculture exhibit multiple characteristic manifestations of sub-object land cover composition, and require subdivision into multiple subclasses for training and classification purposes.

A QuickBird satellite image mosaic that is based on multispectral data captured on several dates in January 2010 and covering the Accra Metropolitan Area was purchased. The multi-spectral data set includes four broad wavebands in the Blue, Green, Red, and Near Infrared (NIR) portion of the electromagnetic spectrum. The multispectral data were utilized for the evaluation of histogram signatures and curve matching. A pan-sharpened version of the same QuickBird image mosaic was used for the manual selection of training and test data. The QuickBird imagery had been georeferenced to the Universal Transverse Mercator map projection by a third-party geoprocessing company at the Standard processing level (CE90 = 23 m; RMSE = 14 m).

3. Methods

The general research approach consisted of sampling pixel groupings or areas of interest (AOIs) representing LCLU types of interest in Accra from a QuickBird multispectral image, evaluating histogram signatures, and testing a simple curve matching routine. Histograms were generated and compared within and between LCLU types. A measure of curve similarity was implemented to quantitatively compare curves from various LCLU polygons. Accuracy of the LCLU classification based on this histogram curve matching approach was compared to results from a nearest neighbor (i.e., minimum distance to means) classifier. Details of the research methods follow.

3.1 Pre-processing

Several pre-processing procedures were conducted on the QuickBird imagery, in addition the geo-processing. A subset image was extracted to avoid clouds and cloud shadows. A

normalized difference vegetation index (NDVI) was derived from uncalibrated digital number (DN) values based on the formula: NDVI = (NIR − Red)/(NIR + Red), as a means for enhancing the contrast between vegetation and non-vegetation surfaces. Through experimentation, we also generated a spectral index that enhances road pavement and other impervious surfaces from soil and vegetation according to the formula: NDRBI = (Red − Blue)/(Red + Blue) and coined it the normalized red-blue index (NDRBI). The two normalized difference spectral indices were used rather than spectral wavebands for most of the study, because of their ability to normalize most of the spatial variability in raw spectral radiance data, such as from atmospheric and view angle effects, and to reduce four highly correlated wavebands into a two-channel data set. Our preliminary analyses of LCLU histogram curves derived from spectral waveband and spectral index data revealed that the spectral index curves were more consistent and characteristic for LCLU types.

3.2 Training and Test Object Histograms

We delineated polygons (i.e., AOIs) representing the five LCLU classes through visual interpretation of the pansharpened QuickBird image and manual digitizing. Since no extant LCLU data sets are available for Accra, delineation of LCLU polygons was guided primarily through visual interpretation, with some knowledge of Accra's landscape and LCLU characteristics gleaned through field reconnaissance. We delineated AOIs manually to include most of an entire LCLU polygon object, erring on the side of excluding pixels from adjacent LCLU polygons (Shandley et al., 1996). Between eight and 15 AOIs were delineated for each LCLU class, ranging from 0.3 to 36 hectares in size. Two or three AOIs were used for training (i.e., a supervised classification context) and the remainder for testing (i.e., accuracy assessment). This yielded between six and 13 test AOIs (polygons) per class, with the predominant urban classes (HSE, LSE and Urban Non-residential) being represented by at least 12 AOIs (as shown in Table 2). While such a sample size is certainly not exhaustive, it represents a reasonable size given: (1) the percentage of study area and number of pixels represented by the sample sets for each class (as illustrated in Table 2), (2) the cumbersome nature of extracting sample sets and testing the curve matching approach (described below) in the absence of custom software tools, (3) the uncertainty in selecting reliable AOIs for specific LCLU categories in the absence of existing maps, and (4) the exploratory nature of our evaluation of the histogram curve matching approach. Pixel samples from each AOI were extracted and ported to a spreadsheet for histogram generation and curve matching. Histograms bin values were normalized by dividing the frequency count for each bin by the total number of pixels in each LCLU AOI.

Our preliminary visual analyses of LCLU histograms revealed the existence of subclass groupings of characteristic signatures. In some cases these subclasses represented different compositions within LCLU polygon and other cases they represented more specific LCLU types within a broader LCLU class to which they were members. In particular for the latter case, specific LCLU subclasses of Urban Non-residential such as Institutional, Industrial, and Commercial types exhibited dissimilar histograms, and were treated as separate spectral-informational classes. This is similar to when selecting and refining training signatures for per-pixel, supervised classification. Training or reference histogram curves were generated by taking the average frequency values at each digital number (DN) bin, or for the Accra QuickBird example, normalized difference index (NDI) bins, for two or three representative curves for each LCLU class or subclass, as illustrated in Figure 2.

3.3 Histogram Curve Matching

A simple measure of similarity for quantitatively comparing and classifying normalized histogram curves of LCLU polygons was utilized. The Histogram Matching Root Sum Squared Differential Area (HMRSSDA) measures histogram similarity by computing the

squared difference at each DN (or NDI bin), summing the squared differences, and taking the square root of this sum, according to the formula:

$$HMRSSDA = 1 - \left(\sum_{i=DN_{min}}^{n=DN_{max}} (FS_i - FR_i)^2\right)^{1/2}$$

where: FS_i = frequency of the subject histogram at i = DN, FR_i = frequency of reference histogram at DN = i, and DN = digital number.

The routine is similar to the spectral curve matching approach utilized by Hamada et al. (2007), which was used successfully to identify invasive plants based on classification of hyperspectral data. Given the exploratory nature of this study, we selected this curve matching measure based on its simplicity and the successful utilization by Hamada and others (2007). For this implementation of HMRSSDA, values are maximized (near 1) when comparing similar histogram curves and approach 0 when they are completely dissimilar. HMRSSDA may be used quantitatively compare curves, or to classify curves against template curves derived from training date. As illustrated in Figure 3, a subject curve is classified according to the LCLU type for which its template curve yields a maximum HMRSSDA value.

4. Results

4.1 Histogram Analysis

Figure 4 depicts the histogram curves for NDVI and NDRBI indices from training data for all five LCLU classes and associated subclasses. Since NDVI varies from low to high with greater amounts of green vegetation cover and NDRBI primarily varies from low to high with greater amounts of impervious material cover, the magnitudes of NDVI and NDRBI histograms for a given LCLU class tend to be on opposite ends of the index ranges. For example, Forest/Natural Vegetation exhibits a high NDVI and low NDRBI signature curve.

The shapes of histograms for each class tend to be consistent for both NDVI and NDRBI, with the exception of Urban Agriculture. Low Socioeconomic Residential (predominantly composed of impervious and soil materials), and Forest (predominantly composed of green vegetation) exhibit normal, highly peaked curves, while High Socioeconomic Residential and Urban Non-Residential subclasses have broad, highly dispersed, and skewed histograms with a dominant mode. Urban Agriculture exhibits a broad right skewed histogram in NDVI and a narrow, Gaussian-like curve with a low magnitude peak in NDRBI. This suggests that the curve matching classification approach relative to a nearest neighbor approach may be advantageous for accurately classifying High Socioeconomic Residential, Urban Non-Residential and Urban Agriculture classes that exhibit broader and more complex distributions.

From a standpoint of between class separability, all curves are characteristic and unique, with the exception of one of the High Socioeconomic Residential and one of the Urban Non-Residential subclasses that were similar for NDRBI. However, the NDVI curves for these same subclasses are unique. Curves of some subclasses from the same parent classes are not always unique, but that does not influence the between-class separability.

4.2 Classification Results

Tables 3 through 5 show accuracy statistics for exploratory classification results based on the histogram curve matching approach for NDVI, NDRBI, and combined NDVI and

NDRBI inputs. The overall agreement is 71.1%, 65.4%, and 73.1%, respectively. Commission errors were generally low for all classes except High Socioeconomic Residential for NDVI and combined NDVI/NDRBI, and Urban Non-residential for NDRBI. Low Socioeconomic Residential and Urban Non-residential had relatively high omission errors in NDVI, while omission errors were highest with NDRBI for High Socioeconomic Residential and Urban Agricultural. When incorporating both spectral indices, the greatest confusion occurred between Low Socioeconomic Residential and Urban Non-residential and between High Socioeconomic Residential and Urban Agriculture classes.

Tables 6 through 8 show classification accuracy statistics for a nearest neighbor classifier applied to within-object mean values for NDVI, NDRBI, and combined NDVI-NDRBI inputs. The overall agreement values are 65.4%, 59.6%, and 73.1%, respectively. Overall accuracy was lower for the nearest neighbor classifier when a single spectral index was incorporated and identical to the curve matching classifier when both indices were utilized. The greatest confusion occurred between High Socioeconomic Residential and Urban Non-residential, the two classes with broadest and least normally distributed histograms.

5. Discussion and Conclusion

The rationale for testing a curve matching approach for within-object pixel classification is that histogram curves may be complex (i.e., non-normal) and characteristic (consistent signatures for particular classes). The results from the empirical evaluation of QuickBird data (GSD = 2.4 m) for LCLU classes in Accra suggest that histograms can have consistently characteristic shapes for particular classes, but do not consistently exhibit complex shapes. Histograms of image brightness values represent the frequency of occurrence of spectral reflectance within an image-derived object, as a function of the material composition within the scene unit associated with an image object. When material composition is diverse and heterogeneous, then histogram distributions can be complex. This is particularly true if a few dominant within-object materials have variable reflectance properties. Spatial arrangements and size variations of sub-object materials are not captured by these histograms. An avenue for future research should be the development of frequency distributions of spatial context measures associated with subobjects and their spatial arrangements within LCLU polygons.

Figures 5 and 6 portray histogram curves from digital airborne multispectral data (GSD = 1 m) for AOIs associated with LCLU and vegetation community types, respectively. The imaged scenes are semi-arid suburban and rural shrubland landscapes (respectively) near San Diego, California, USA. The mean curves shown in Figure 5 for six LCLU types were extracted from the NIR waveband of an ADS-40 digital image and exhibit a high degree of shape complexity and most have multiple modes. Conversely, the mean curves of six vegetation community types extracted from the Red waveband of an ADAR 5500 multispectral image of an undeveloped rural shrubland landscape exhibit narrow, normally distributed curves with minimal complexity. These “pilot study” curves, in conjunction with those from the Accra QuickBird imagery suggest that curve complexity and therefore, the potential of curve matching classifiers depend on landscape structure, classification objective, and the spatial resolution of the input image data.

The curve matching approach to classifying multi-pixel objects corresponding to LCLU units is promising. While the HMRSSDA classifier yielded slightly higher to identical accuracy relative to a nearest neighbor classifier, more extensive sample sets and tests for varying image spatial resolutions, landscape types and LCLU schemes should be incorporated in future studies to fully determine its effectiveness. The curve matching approach seems to be most effective when the mean, standard deviation and other

parametric statistical moments do not sufficiently describe a complex, non-normal frequency distribution.

The classification measure that was tested, HMRSSDA, is based on a very simplistic measure of curve similarity. More robust measures of curve similarity such as hyperdimensional angle mapper and spectral information divergence, utilized for hyperspectral curve matching (van der Meer, 2006), should be evaluated for histogram curve matching purposes. In addition to providing a classification metric, HMRSSDA and other curve similarity measures may be useful as quantitative measures for assessing whether or not within-object pixel groups from a given LCLU class have characteristic signatures. Such measures may also be used as separability metrics when selecting and grouping training histograms for a given class, such as when developing subclass signatures. More generalized LCLU classes may be composed of several spectral-informational subclasses that have unique histogram shapes, whereas the mean curve for the entire sample of AOIs for the general class may not be characteristic or unique.

As stated early in this paper, the premise of the curve matching classification approach is that image objects have first been delineated, either through image segmentation (most commonly), or by incorporating extant digital representations of field or parcel boundaries. For the curve matching classification to be successful, image segments must be sufficiently large to capture the characteristic variability of image brightness values associated with a given class. If delineated too small, the distributions may be more representative of homogeneous subobjects having histogram signatures that are different from the characteristic curve of an entire LCLU unit.

Humans conducting manual interpretation for LCLU mapping tend to integrate the object delineation and classification tasks when mapping LCLU polygons. In other words, they are generally cognizant of the LCLU class membership when delineating (e.g., heads-up digitizing) the boundary of a polygon. This suggests that histogram curve template matching may be useful not only for classifying pixel groups belonging to an image object, but also in image segmentation when delineating image objects that correspond to LCLU boundaries.

The next steps for follow-on research will be to: (1) implement the curve matching approach into image processing software to enable more efficient and robust generation of training curves and calculation of histogram matching scores, (2) generate a more exhaustive data set (i.e., larger sample size) and evaluate the curve matching approach for one or more study areas for which LCLU data are readily available, (3) examine the relationship between image spatial resolution and within-object frequency signatures, and (4) test other measures of curve similarity (i.e., other than HMRSSDA).

Acknowledgments

Partial funding for this study was provided by the National Institute of Child Health and Human Development – Grant no. R01 HD054906-01 (John Weeks, principal investigator). Lloyd (Pete) Coulter provided image processing support.

References

Berberoglu S, Lloyd CD, Atkinson PM, Curran PJ. The integration of spectral and textural information using neural networks for land cover mapping in the Mediterranean. Comp. & Geosci. 2000; 26:385–396.

Blaschke T. Object based image analysis for remote sensing. ISPRS J. of Photogrammetry & Remote Sensing. 2009; 65:2–16.

Burnett C, Blaschke T. A multi-scale segmentation/object relationship modeling methodology for landscape analysis. Ecological Modelling. 2003; 168(3):233–249.

Coulter L, Stow D, Anguelova Z, Hamada Y. Monitoring Habitat Preserves in Southern California Using High Spatial Resolution Multispectral Imagery. Environ. Monitoring & Management. 2009; 152:343–356.

Cheng Y-C, Chen S-Y. Image classification using color, texture and regions Image classification using color, texture and regions. Image & Vision Computing. 2003; 21:759–776.

Dean AM, Smith GM. An evaluation of per-parcel land cover mapping using maximum likelihood class probabilities. Intl. J. of Remote Sensing. 2003; 24:2905–2920.

Dey, V.; Zhang, Y.; Zhong, M. A review on image segmentation techniques with remote sensing perspective. In: Wagner, W.; Székely, B., editors. ISPRS TC VII Symposium – 100 Years ISPRS; IAPRS; July 5–7, 2010; Vienna, Austria. 2010. p. 31-42.

Ghana Statistical Services. Accra, Ghana: Ghana Statistical Services; 2002. 2000 Population and Housing Census: Summary Report of Final Results; p. 62

Hamada Y, Stow D, Coulter L, Jafolla J, Hendricks L. Mapping tamarisk species (Tamarix spp.) in riparian habitats of southern California using high spatial resolution hyperspectral imagery. Remote Sensing of Environment. 2007; 109:237–248.

Haralick RM, Shapiro L. Image segmentation techniques. Computer Vision Graphics & Image Processing. 1985; 29:100–132.

Hay, GJ.; Castilla, G. Geographic Object-Based Image Analysis (GEOBIA): Paradigm shift or new methods?. In: Blaschke, T.; Lang, S.; Hay, GJ., editors. Object-Based Image Analysis – spatial concepts for knowledge-driven remote sensing applications. Springer-Verlag; 2008. p. 91-110.

Kruse FA, Lefkoff AB, Boardman JW, Heidebrecht KB, Shapiro AT, Barloon PJ, Goetz AFH. The spectral image processing system (SIPS)—interactive visualization and analysis of imaging spectrometer data. Remote Sensing of Environ. 1993; 44:145–163.

Landgrebe DA. The development of a spectral-spatial classifier for earth observational data. Pattern Recognition. 1980; 12:165–175.

Lippitt C, Coulter L, Lamantia-Bishop J, Freeman J, Pang W, Stow D. The effect of input data transformations on object-based image analysis. Intl. J. of Remote Sensing. in press.

Lloyd CD, Berberoglu S, Curran PJ, Atkinson PM. A comparison of texture measures for the per-field classification of Mediterranean land cover. Intl. J. of Remote Sensing. 2004; 25:3943–3965.

Mason DC, Corr DG, Cross A, Hogg DC, Lawrence DH, Petrou M, Tailor AM. The use of digital map data in the segmentation and classification of remotely-sensed images. Intl. J. of Geog. Info. Sys. 1988; 2:195–215.

Neubert, M.; Herold, H.; Meinel, G. Assessing image segmentation quality: Concepts, methods and application. In: Blaschke, T.; Lang, S.; Hay, GJ., editors. Object Based Image Analysis. Heidelberg, Berlin, New York: Springer; 2008. p. 760-784.

Pedley MI, Curran PJ. Per-field classification: an example using SPOT HRV imagery. Intl. J. of Remote Sensing. 1991; 12:2181–2192.

Saykol E, Gudukbay U, Ulusoy O. A histogram-based approach for object-based query-by-shape-and-color in image and video databases. Image and Vision Computing. 2005; 23:1170–1180.

Schiewe, J. Segmentation of high-resolution remotely sensed data concepts, applications and problems; Joint ISPRS Commission IV Symposium: Geospatial Theory, Processing and Applications; 9–12 July 2002; 2002.

Shackelford AK, Davis CH. A combined fuzzy pixel-based and object-based approach for classification of high-resolution multispectral data over urban areas. IEEE Trans. on Geoscience & Remote Sensing. 2003; 41:2354–2364.

Shandley J, Franklin J, White T. Testing the Woodcock-Harward image segmentation algorithm in an area of southern California chaparral and woodland vegetation. Intl. J. of Remote Sensing. 1996; 17:983–1004.

Stow D, Lippitt C, Lopez A, Hinton S, Weeks J. Object-based classification of residential land use within Accra, Ghana based on QuickBird satellite data. Intl. J. of Remote Sensing. 2007; 28:5167–5173.

Stow D, Lippitt C, Weeks J. Geographic object-based delineation of neighborhoods of Accra, Ghana using QuickBird satellite imagery. Photogrammetric Eng. & Remote Sensing. 2010; 76:907–914.

Swain MJ, Ballard DH. Color indexing. International Journal of Computer Vision. 1991; 7:11–32.

van der Meer F. The effectiveness of spectral similarity measures for the analysis of hyperspectral imagery. Intl. J. of Appl. Earth Observation & Geoinformation. 2006; 8:3–17.

Weeks JR, Hill AG, Getis A, Stow D. Ethnic residential patterns as predictors of intra-urban child mortality inequality in Accra, Ghana. Urban Geography. 2006; 27:526–548. [PubMed: 19816546]

Weeks JR, Hill AG, Stow D, Getis A, Fugate D. Can we spot a neighborhood from the air? Defining neighborhood structure in Accra, Ghana. GeoJournal. 2007; 69:9–22. [PubMed: 19478993]

Woodcock CE, Harward J. Nested-hierarchical scene models and image segmentation. Intl. J. of Remote Sensing. 1992; 13:3167–3187.

Zhang H, Gao W, Chen X, Zhao D. Object detection using spatial histogram features. Image & Vision Computing. 2006; 24:327–341.

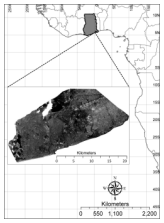

Figure 1.
Study area map of Accra, Ghana with QuickBird satellite image mosaic (Red waveband).

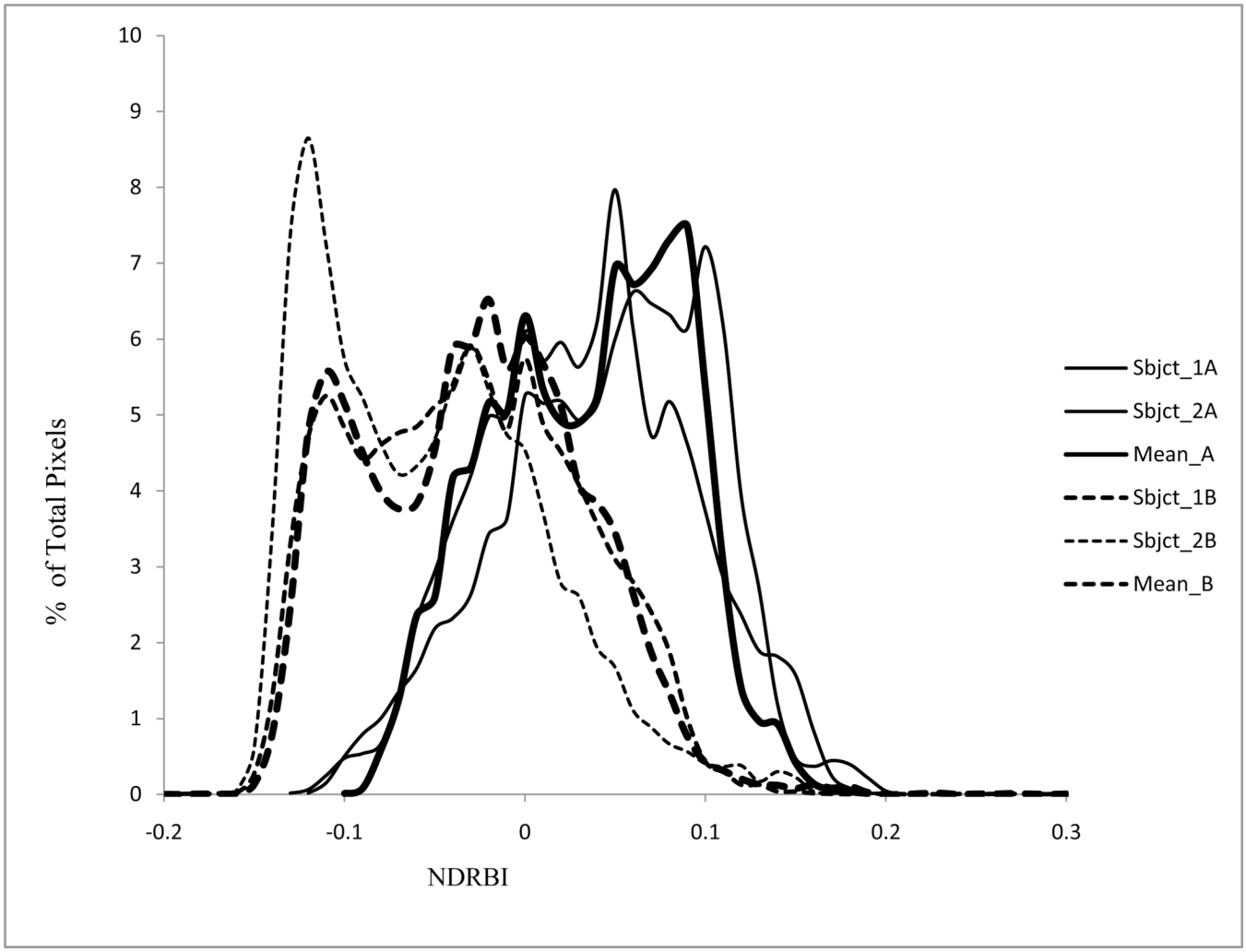

Figure 2.
Example of training AOIs and mean histogram curves for two subclasses of the Urban Non-residential class derived from the QuickBird normalized difference red-blue index (NDRBI) image.

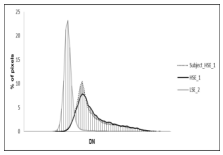

Figure 3.
Schematic of the histogram curve matching approach illustrating a subject histogram for a High Socioeconomic Residential (HSE) object compared to training class histograms for HSE and Low Socioeconomic (LSE) classes. Shaded areas depict differences between the subject and mean curves.

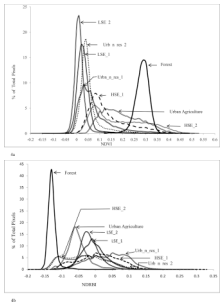

Figure 4.
Training (mean) histogram curves for all classes and subclasses. a. NDVI and b. NDRBI.

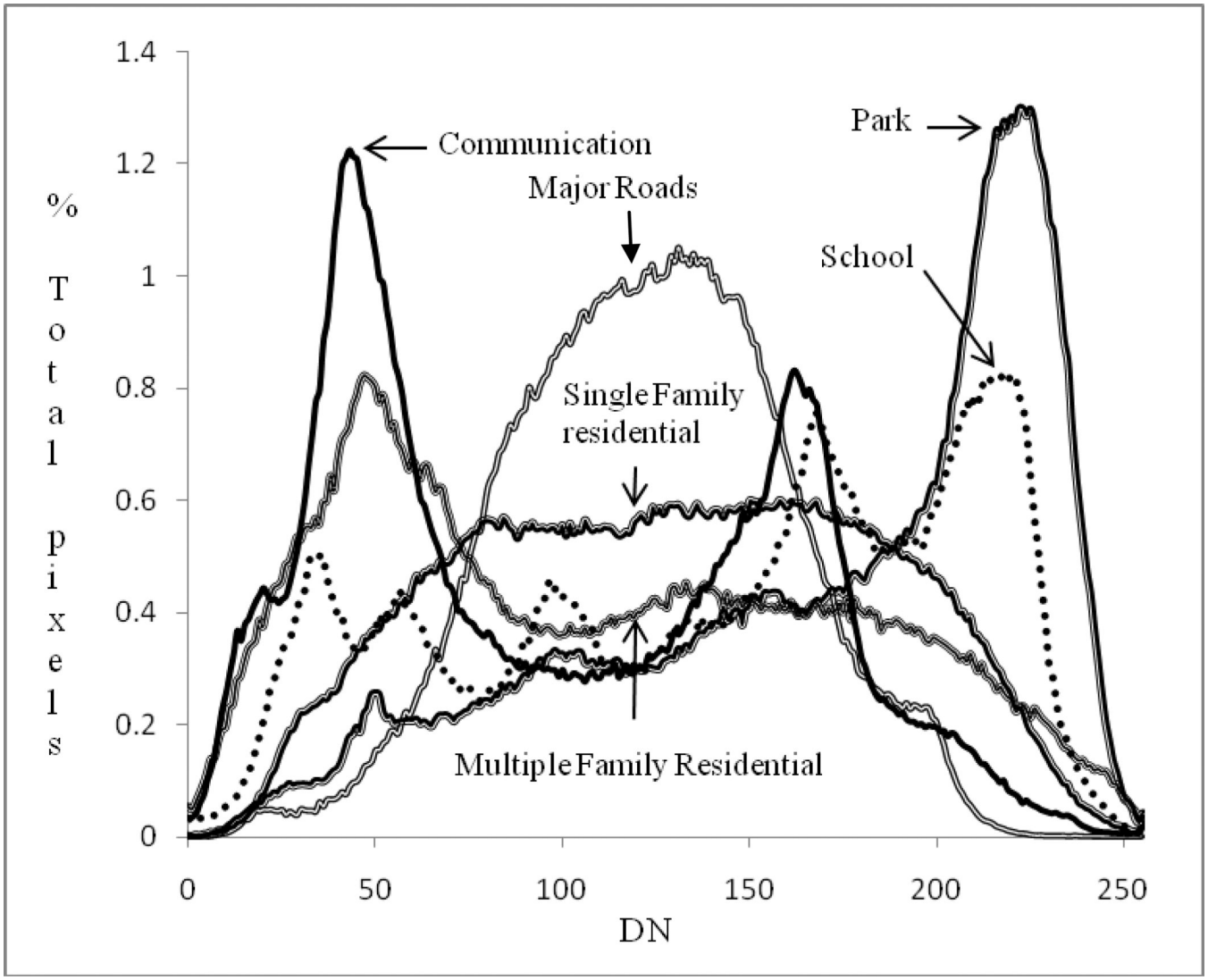

Figure 5.
Histogram curves for land cover and land use AOIs derived from NIR waveband of ADS-40 (GSD = 1 m) image of a portion of San Diego, California, USA.

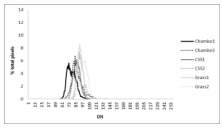

Figure 6.
Histogram curves for vegetation community AOIs derived from Red waveband of ADAR 5500 (GSD = 1 m) image near San Diego, California, USA.

Table 1

Land cover and land use classes with descriptions.

Land Cover/Land Use Classes	Class Descriptions
Forest (and other natural vegetation)	Lush vegetation mostly forest on the outskirts of city, and wetland vegetation along river and tidal slough areas
High Socio-Economic Residential (HSE)	Moderate to large size structures, lush landscape vegetation, mostly paved streets, more organized neighborhood structure
Low Socio-Economic Residential (LSE)	Small informal dwellings to large building compounds, minimal landscape vegetation, mostly unpaved streets, often chaotic settlement pattern
Urban Non-residential	Commercial, industrial and institutional land uses; large buildings with parking lots, some landscape vegetation
Urban Agriculture	Vegetated and fallow plots with fairly rectangular shapes

Table 2

Training and test areas of interest (AOIs) for evaluation of histogram curve matching classification by land cover and land use classes.

Land Cover/ Land Use Classes	No. Train AOIs	No. Pixels Train AOIs	Area Covered by Train AOIs	% Study Area Train AOIs	No. Test AOIs	No. Pixels Test AOIs	Area Covered by Test AOIs	% Study Area Test AOIs
Forest/Other Natural Vegetation	3	40686	23.4 ha	0.09%	6	62525	36.0 ha	0.14%
High Socio-Economic Residential (HSE)	5	98188	56.6 ha	0.23%	12	201815	116.3 ha	0.46%
Low Socio-Economic Residential (LSE)	5	178210	102.7 ha	0.41%	12	325972	187.8 ha	0.75%
Urban Non-residential	5	145719	83.9 ha	0.34%	13	231016	133.0 ha	0.53%
Urban Agriculture	2	9383	5.4 ha	0.02%	9	35596	20.5 ha	0.08%

Study area = 25054.91 ha

Table 3

Classification accuracy matrix for HMRSSDA classification of NDVI

Reference Data							
		Forest	**HSE**	**LSE**	**Urban Non-Residential**	**Urban Agriculture**	**Total**
Histogram Classification	Forest	6	0	0	0	0	6
	HSE	0	12	0	5	1	18
	LSE	0	0	7	2	0	9
	Urban Non-Residential	0	0	5	5	1	11
	Urban Agriculture	0	0	0	1	7	8
	Total	6	12	12	13	9	52

Overall Accuracy: 37 ÷ 52 = 71.2%

Table 4

Classification accuracy matrix for HMRSSDA classification of NDRBI

Reference Data							
		Forest	**HSE**	**LSE**	**Urban Non-Residential**	**Urban Agriculture**	**Total**
Histogram Classification	Forest	6	0	0	0	0	6
	HSE	0	6	3	3	3	15
	LSE	0	0	9	0	1	10
	Urban Non-Residential	0	6	0	10	2	18
	Urban Agriculture	0	0	0	0	3	3
	Total	6	12	12	13	9	52

Overall Accuracy: 34 ÷ 52 = 65.4%

Table 5

Classification accuracy matrix for HMRSSDA classification of NDVI & NDRBI

		Reference Data					
		Forest	**HSE**	**LSE**	**Urban Non-Residential**	**Urban Agriculture**	**Total**
Histogram Classification	Forest	6	0	0	0	0	6
	HSE	0	12	0	5	5	22
	LSE	0	0	8	0	0	8
	Urban Non-Residential	0	0	4	8	0	12
	Urban Agriculture	0	0	0	0	4	4
	Total	6	12	12	13	9	52

Overall Accuracy: 38 ÷ 54 = 73.1%

Table 6

Classification accuracy matrix for nearest neighbor classification of NDVI

Reference Data							
		Forest	**HSE**	**LSE**	**Urban Non-Residential**	**Urban Agriculture**	**Total**
Nearest Neighbor Classification	Forest	6	0	0	0	1	7
	HSE	0	12	0	7	3	22
	LSE	0	0	7	0	0	7
	Urban Non-Residential	0	0	5	5	1	11
	Urban Agriculture	0	0	0	1	4	5
	Total	6	12	12	13	9	52

Overall Accuracy: 34 ÷ 52 = 65.4%

Int J Appl Earth Obs Geoinf. Author manuscript; available in PMC 2013 April 1.

Table 7

Classification accuracy matrix for nearest neighbor classification of NDRBI

Reference Data							
		Forest	**HSE**	**LSE**	**Urban Non-Residential**	**Urban Agriculture**	**Total**
Nearest Neighbor Classification	Forest	6	0	0	0	0	6
	HSE	0	5	5	3	0	13
	LSE	0	2	6	1	1	10
	Urban Non-Residential	0	5	1	8	2	16
	Urban Agriculture	0	0	0	1	6	7
	Total	6	12	12	13	9	52

Overall Accuracy: 31 ÷ 52 = 59.6%

Table 8

Classification accuracy matrix for nearest neighbor classification of NDVI & NDRBI

Reference Data							
		Forest	**HSE**	**LSE**	**Urban Non-Residential**	**Urban Agriculture**	**Total**
Nearest Neighbor Classification	Forest	6	0	0	0	0	6
	HSE	0	12	0	8	2	22
	LSE	0	0	11	2	0	13
	Urban Non-Residential	0	0	1	3	1	5
	Urban Agriculture	0	0	0	0	6	6
	Total	6	12	12	13	9	52

Overall Accuracy: 38 ÷ 54 = 73.1%

Int J Appl Earth Obs Geoinf. Author manuscript; available in PMC 2013 April 1.